Biosensors and Bioelectronics xxx (xxxx) xxx

Contents lists available at ScienceDirect

Biosensors and Bioelectronics

journal homepage: http://www.elsevier.com/locate/bios

Smartphone-integrated urinary CTX-II immunosensor based on wavelength filtering from chromogenic reaction

Saemi Kim [1], Hyeong Jin Chun [1], Kyung Won Lee, Hyun C. Yoon [*]

Department of Molecular Science and Technology, Ajou University, Suwon, 16499, South Korea

ARTICLE INFO

Keywords:
Smartphone-based biosensor
Point-of-care testing (POCT)
Count-based analysis
Filtering effect
uCTX-II detection
Artificial urine

ABSTRACT

The integration of smart IT devices and biochemical assays with optical biosensing technology facilitates the development of efficacious optical biosensors for many practical diagnostic fields, owing to their minimized use of high-technical electronic components and simple operation. Herein, we introduced a simple optical biosensing system based on the specific wavelength filtering principle and count-based analysis method. The developed system uses a smartphone with a paper-based signal guide and a biosensing channel. The paper-based signal guide was prepared by printing red patterns of various brightness on a black background. Given that a blue product is generated as a result of horseradish peroxidase (HRP)-based enzymatic reaction in the biosensing channel, the channel could be used as a blue filter that absorbs red light. When red light reflected from the red pattern is absorbed by the channel, the pattern appears black. As such, the color of the patterns is assimilated with the black background, so it seems to disappear. Consequently, the amount of blue product relative to the concentration of the target analyte can be measured by counting the number of observed patterns on the paper-based signal guide. In this study, the concentration of urinary C-telopeptide fragment of type II collagen (uCTX-II, 0–10 ng/mL) was measured using the developed system without complicated equipment. In addition, the quantitative analysis of uCTX-II in the real urine sample was successfully performed. Therefore, we expect that the developed optical transducing system could be practically used for point-of-care testing (POCT) diagnosis under resource-limited environmental conditions.

1. Introduction

Rapid, accurate and simple operating diagnostic devices for point-of-care testing (POCT) are crucial in clinical and research fields. In this regard, various approaches have been proposed to improve the reliability and availability of POCT devices by integrating multiple functions and diagnostic principles. Based on this approach, the diagnostic test time can be reduced, which improves the treatment efficiency of the patient and simplifies the acquisition of patient information (Uys et al., 2009). Although high-end biosensing principles exhibit high reliability for disease evaluation, most of these techniques are conducted by skilled technicians in a medical or laboratory setting. In addition, the diagnostic instrument is expensive and typically requires a high-voltage power supply. Thus, the complexity of technologies is inconvenient for the users or patients (Klostranec and Chan, 2006; Mabey et al., 2004; Peeling and Mabey, 2010).

Recently, various researchers have attempted to develop the practically useful diagnostic device by using the smart information technology (IT) device as a POCT device based on their useful high-end technology with versatile functionalities such as embedded physical sensors and related high computing capability (Guo, 2016, 2017). The high-end electronic components facilitate the minimization and simplification of biosensors by integrating the smart IT device and biochemical principles. The various functionalities of smart IT devices facilitate the automatic calculation and display of data as well as simple operation, which reduces the evaluation time and biosensor cost. Thus far, many types of smart IT device-based biosensors have been reported as POCT devices for the detection of microscale bio-components, integrated with the functionalities of smartphones (Chun et al., 2014; Coleman et al., 2019; Coskun et al., 2013; Huang et al., 2018; Kang et al., 2017; Kim et al., 2015; Ozcan, 2014; Park et al., 2015; Shen et al., 2012; Soni et al., 2018; Vashist et al., 2015; Wang et al., 2017; Wei et al., 2017; Xie et al., 2018; Xu et al., 2018; Yang et al., 2019; Yu et al., 2014). Although previous studies have demonstrated high sensitivity and

* Corresponding author.
E-mail address: hcyoon@ajou.ac.kr (H.C. Yoon).
[1] The authors wish it to be known that, in their opinions, Saemi Kim, Hyeong Jin Chun should be regarded as joint First Authors.

https://doi.org/10.1016/j.bios.2019.111932
Received 24 July 2019; Received in revised form 25 November 2019; Accepted 26 November 2019
Available online 27 November 2019

portability, the developed principles still required an external apparatus to incorporate the additional functionality with a smart IT device, which leads to inconvenience and loss of portability.

To resolve the limitations of previously developed smartphone-based biosensors, Chun et al. introduced a naked eye detection system by integrating a simple enzyme-based colorimetric biosensing application with the selective light absorption and wavelength filtering phenomena (Chun et al., 2018). To successfully integrate sensitive optical analytic techniques with a smartphone, a new optical biosensing system using a smartphone and a liquid crystal display (LCD) panel was utilized. In this system, the LCD panel of a computer monitor was used as a light source and the signal guide to serve the optical signal, and a smartphone was used as an optical receiver and for signal display. The appearance of the signal guide on the LCD panel was registered with a smartphone via a transparent biosensing channel with a blue product induced by a chromogenic reaction. Using this sensing system, an intuitive analysis was possible by counting the number of figures observed in the signal guide without sophisticated optical equipment. However, this system is limited by a lack of portability because an LCD panel was used as the light source and the signal guide.

To overcome this limitation, we fabricated a new signal guide that replaces the LCD panel with a paper-based signal guide. Given that the signal guide was simply printed on paper, there are numerous associated advantages such as low cost, ease of manufacture, and mass-production (Zeng et al., 2019a, 2019b; Guo and Ma, 2017). In addition, by using a smartphone flash as a light source and a smartphone camera as an optical receiver and signal display, an optical signal can be analyzed with the function of smartphone and very simple components. To introduce count-based analysis in this sensing system, selective light absorption and specific wavelength filtering phenomena were employed. A specific color-filter can selectively transmit light of the same color as the filter and absorb other light. For example, when the blue and red letters printed on a paper are observed through a blue filter, the blue letter is visible because the blue light from the letter can pass through the filter. However, the red letter appears black because the red light is absorbed by the filter. Therefore, when the color of the pattern printed on the paper-based signal guide is matched to the absorption wavelength of the biosensing channel in which color development is induced by a target molecule, the patterns can seem to disappear, similar to the case when the background color of the pattern is black. If several patterns with various intensities of the matched color are printed on a paper-based signal guide to produce discriminable optical signals, the number of observed patterns would be sequentially changed by the amount of color-product generated in the biosensing channel. Based on the developed biosensing principle, a quantitative analysis could also be performed by counting the number of observed patterns in the signal guide (Fig. 1).

To successfully validate the analytical performance of the developed biosensing system, an HRP-based colorimetric assay was introduced. The HRP-linked immunoassay was performed to detect the presence of urinary C-telopeptide fragment of type II collagen (uCTX-II), which is one of the biomarkers of osteoarthritis (Garnero et al., 2005; Kong et al., 2006; Reijman et al., 2004). To fabricate a target-specific biosensing channel surface for each biochemical assay, the polydopamine modification technique was used with a polydimethylsiloxane (PDMS) biosensing channel to facilitate the stable immobilization of peptide (Han et al., 2014; Lee et al., 2007; Park et al., 2017). Based on the developed optical biosensing system, uCTX-II was efficiently quantified without additional apparatus to transduce an optical signal. Thus, the assay is suitable for POCT-based uCTX-II analysis. The details of the biosensing principle and analytical approaches are reported herein.

2. Experimental

2.1. Reagents and apparatus

Dopamine hydrochloride, tris(hydroxymethyl)aminomethane, ethanolamine (EA), glucose, albumin, calcium chloride, magnesium chloride, sodium chloride, sodium sulfate, sodium citrate, sodium oxalate, potassium phosphate, potassium chloride, ammonium chloride, urea, creatine and tryptic soy broth were purchased from Sigma-Aldrich. The fragments and amine-terminated PEG_4-EKGPDP were provided by Peptron Inc. The uCTX-II ELISA kit and sCTX-II ELISA kit, that include horseradish peroxidase-labeled monoclonal anti-uCTX-II antibody (HRP-Ab) and 3,3′,5,5′-tetramethylbenzidine (TMB), were obtained from Immunodiagnostic Systems Inc. Bovine serum albumin (BSA) was obtained from BioWorld. Phosphate buffered saline (PBS) was purchased from Thermo Scientific. The Sylgard® 184 silicone elastomer kit was purchased from Dow Corning. For the reaction solution, artificial urine solution (AUS) containing calcium chloride (0.651 g/L),

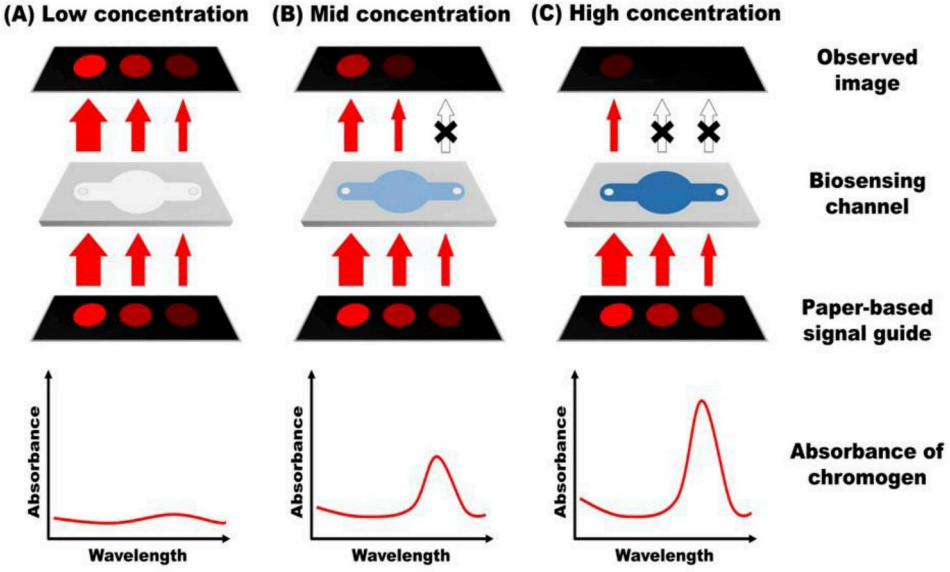

Fig. 1. Basic concept of the count-based analysis. The number of observed patterns depends on the amount of the blue-colored product generated by the chromogenic reaction in the biosensing channel (A) low concentration, (B) Mid concentration and (C) High concentration of the chromogenic product. (For interpretation of the references to color in this figure legend, the reader is referred to the Web version of this article.)

magnesium chloride (0.651 g/L), sodium chloride (4.6 g/L), sodium sulfate (2.3 g/L), sodium citrate (0.65 g/L), sodium oxalate (0.023 g/L), potassium phosphate (2.8 g/L), potassium chloride (1.6 g/L), ammonium chloride (1.0 g/L), urea (25.0 g/L), creatine (1.1 g/L) and tryptic soy broth (10.0 g/L) was used. Double distilled and deionized water (DDW) with a specific resistance greater than 18 MΩ cm was used in all experiments.

2.2. Preparation of the paper-based signal guide

The color printed on the paper is usually determined based by the CMYK (cyan, magenta, yellow and black) combination. Therefore, the CMYK color model was used to fabricate the paper-based signal guide. In thus color model, the intensity of red can be adjusted by changing the C value. As the C value increases from 0 to 100, the color changes from bright red to dark red. The K value that represents black is involved in color saturation and brightness. Based on these features, we fabricated a signal guide consisting of various red patterns and a black background. Each pattern represented the red color using a combination of C, M, Y, and K, possessing the same value of M, Y, and K (with the exception of C). To represent a dark color, the background area of the patterns was set to have relatively high C and K values compared to the patterns.

2.3. Fabrication and surface modification of the biosensing channel

The biosensing channel was fabricated with polydimethylsiloxane (PDMS) at the top and polyethylene terephthalate (PET) film at the bottom. The mold for casting the PDMS was made of acrylic. The PDMS monomer and its curing agent were mixed at a volume ratio of 10:1. The mixture of PDMS was poured onto the acrylic mold and cured at 70 °C for 1 h. After the PDMS was detached from the acrylic mold, each PDMS channel was punched to make an inlet and an outlet hole and washed with DDW. Each fabricated PDMS substrate has one channel which has a bioreaction region in the center and contains two holes (inlet and outlet) to inject the solution. To prevent solution leaks from the channel, the PDMS channel was combined with PET film containing an adhesion on one side. The volume of each channel was 250 μL. To construct the biorecognition layer on the surface of the biosensing channel, a polydopamine coating method was used. Specifically, 2 mg/mL of dopamine hydrochloride dissolved in 10 mM Tris-HCl buffer (pH 8.5) was immediately injected into the biosensing channel. After reacting for 16 h, the channel was washed with DDW and stored at 4 °C until further biomolecular modification.

2.4. Fabrication of the biorecognition layer for competitive immunoassay

To construct the biorecognition layer for the uCTX-II competitive immunoassay, 80 μg/mL of amine-terminated PEG_4-EKGPDP peptide was injected in the channel coated with polydopamine and reacted for 3 h. PEG_4-EKGPDP could be immobilized on the sensing surface by the reaction between its amine group and the polydopamine of the sensing surface. Next, 20 mM EA and 0.1% BSA were reacted for 30 min each to block the non-immobilized region of PEG_4-EKGPDP.

2.5. uCTX-II competitive immunoassay

The competitive reaction of uCTX-II and PEG_4-EKGPDP was used for the uCTX-II assay. In this regard, various concentrations of uCTX-II (0, 2.5, 5, 7.5 and 10 ng/mL, in 0.1 M PBS) and HRP-conjugated anti-CTX-II antibodies were mixed in the ratio of 3:1 and reacted for 60 min. This mixture was injected to the channel where the PEG_4-EKGPDP was immobilized and reacted for 30 min (Han et al., 2014; Park et al., 2017). After washing with PBS, TMB reagent was added and incubated for 10 min (Fig. S1, supplementary information). The intensity of the color development was evaluated using the naked eyes and absorbance measurement. The appearance of the signal guide that changed due to the blue-colored biosensing channel was registered using the smartphone camera, and images were acquired every minute for 10 min. Finally, the number of observed patterns in the signal guide with the sketch filter effect was counted.

3. Results and discussion

3.1. Signaling principle of the developed smartphone-based optical sensing system using filtering effect

The basic principle of this investigation is the color-filtering effect based on color development induced by an enzyme-mediated chromogenic reaction. To effectively perform an enzyme-based catalytic reaction, the sensitive chromogenic reagents (HRP and TMB) were selected. Generally, the TMB substrate is oxidized and converted into a blue-colored product in the presence of hydrogen peroxide. The oxidized TMB substrate maximally absorbs 652 nm wavelength, which is in the red region of the spectrum (Szili et al., 2011; Tatzber et al., 2003). Regarding these optical properties, the presented HRP-based catalytic activity with a blue final product could be used as a red-specific optical filter. To perform quantitative analysis using selective light absorption of the biosensing channel, a paper-based signal guide consisting of red patterns with various brightness on a black background was used for signal analysis. Due to the generated blue-colored product in the biosensing channel, the signal guide could be observed due to the absorbed red light. Therefore, the number of observed red patterns on the signal guide disappeared proportionally to the amount of the blue-product generated in the biosensing channel, i.e. with an increase of the amount of red light absorbed by the biosensing channel.

In this study, to evaluate the applicability of the developed analysis principle to biosensing, uCTX-II was chosen as a target model. Given that uCTX-II has a monomeric epitope, it should be detected using a competitive immunoassay (Birmingham et al., 2006; Eyre et al., 2008; Kim et al., 2013). To achieve this requirement, the surface of the biosensing channel was immobilized with PEG_4-EKGPDP, which competitively binds to the anti-uCTX-II antibody with the uCTX-II fragment. As the concentration of uCTX-II increases, more anti-uCTX-II antibodies bound with uCTX-II fragments, thereby reducing the amount of anti-uCTX-II antibodies that could react with PEG_4-EKGPDP on the sensing surface. At this time, since the anti-uCTX-II antibody was labeled with HRP, it could induce a chromogenic reaction of TMB. That is, HRP-labeled anti-uCTX-II antibodies (HRP-Abs), which remained on the sensing surface after washing by binding with PEG_4-EKGPDP, could induce the oxidation and the chromogenic reaction of TMB. Consequently, the amount of TMB color development, which is inversely proportional to the concentration of uCTX-II, would be measured by counting the number of observed red patterns.

3.2. Fabrication of the paper-based signal guide

To fabricate the paper-based signal guide, it is necessary to adjust the color of the patterns present in the signal guide. This implies that the specific wavelength filtering effect of the blue-colored product produced by TMB should be confirmed first. To verify the specific wavelength filtering effect of the color-developed biosensing channel by enzymatic chromogenic reactions, various colored letters (red, green, blue, cyan, magenta, yellow and black) were printed on paper, and each color was observed according to the presence or absence of the biosensing channel (Fig. 2).

For the paper with the white background, most of the letters were observed in the original color. However, due to the absorption of the red light by the biosensing channel, the “R” and “M” were observed as black instead of as red (Fig. 2A). Therefore, we hypothesized that if we used the black color as a background, the “R” and “M” would disappear. Based on this hypothesis, the paper with the black background was observed via the blue-colored biosensing channel. As shown in Fig. 2B,

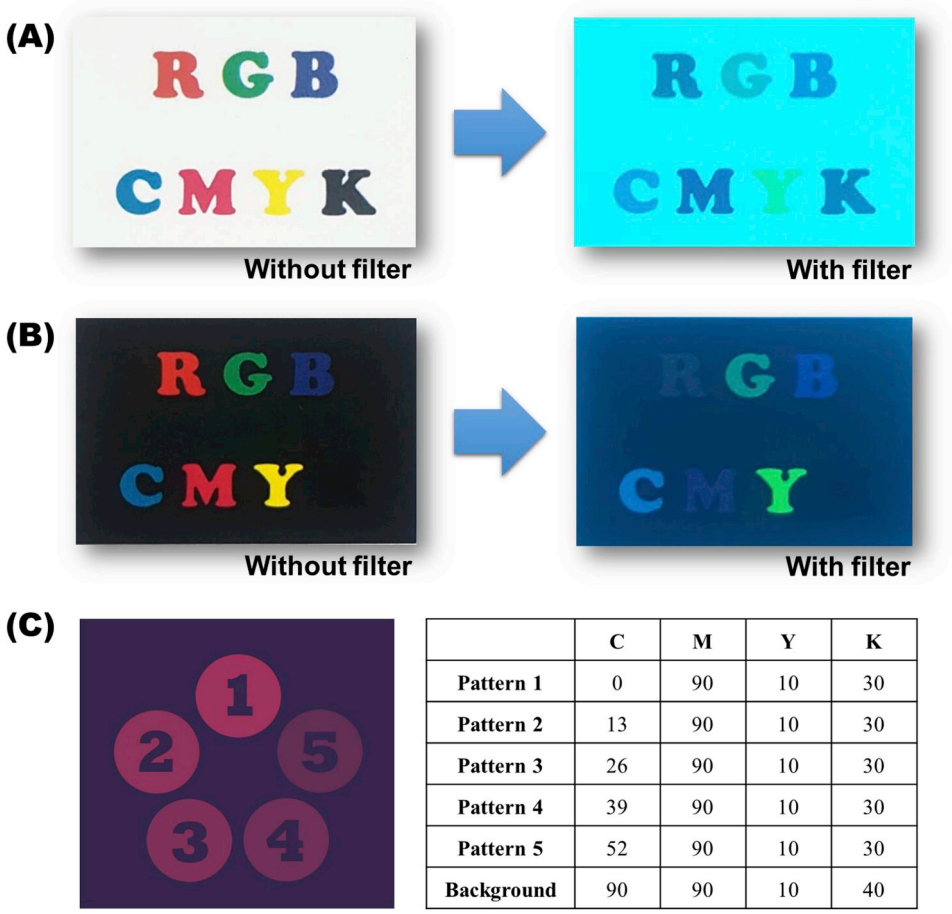

	C	M	Y	K
Pattern 1	0	90	10	30
Pattern 2	13	90	10	30
Pattern 3	26	90	10	30
Pattern 4	39	90	10	30
Pattern 5	52	90	10	30
Background	90	90	10	40

Fig. 2. Verification of the wavelength filtering effect of the blue-colored biosensing channel (A) white background and (B) black background. (C) The image of the designed paper-based signal guide (left) according to the wavelength filtering effect and CMYK value of each pattern (right). (For interpretation of the references to color in this figure legend, the reader is referred to the Web version of this article.)

the "R" and "M" on the black background are not observed. To compare the change of color intensity based on objective quantification, the RGB values of all the letters were analyzed using ImageJ software (Fig. S2). The results show that the R values of all the letters were significantly reduced, indicating that the blue-colored biosensing channel could selectively absorb the red light. These results suggest that this biosensing channel can be used as an optical filter for the filtering effect. Therefore, it was confirmed that the use of the blue-colored biosensing channel as the filter that absorbed the red light and the use of the signal guide with red patterns on the black background were appropriate. Based on these results, the paper-based signal guide was prepared (Fig. 2C). The signal guide consists of five patterns with different red intensities (Fig. 2C, left). The color of each pattern was adjusted using a combination of C, M, Y, and K with the same value of M, Y, and K (with the exception of C). The C value of each red pattern was adjusted at specific intervals (Fig. 2C, right). The lower the C value, the brighter the redness of the pattern, so more red light is reflected. Since the amount of absorbed red light depends on the generated amount of the chromogenic product in the biosensing channel, the number of observed red patterns would be changed accordingly.

3.3. Optimization of the biosensing condition

In this study, the signal for the increase in the color intensity and the absorbance of the blue product induced according to the concentration of uCTX-II in the biosensing channel could be transduced by the number of remaining red patterns present in the signal guide. In other words, to perform the accurate uCTX-II biosensing to facilitate quantitively analysis, the disappearance of red patterns should represent a change in the concentration of the uCTX-II with high sensitivity. Therefore, the concentration of the immobilized PEG_4-EKGPDP peptide and the reaction time of a uCTX-II immunoassay should be optimized because these factors are closely related to the rate of generation of the blue-colored final product in the biosensing channel. To compare the color-development produced by the PEG_4-EKGPDP, many types of biosensing channels that were immobilized with various concentration of PEG_4-EKGPDP (0–100 μg/mL) were prepared. HRP-Ab that can recognize the EKGPDP was applied to each prepared biosensing channel and test images were registered every 1 min up to 10 min. The results of visual observations and absorbance measurements confirmed that the amount of color development increased in proportion to the concentration of PEG_4-EKGPDP and the reaction time of TMB (Figs. 3A and S3).

For the case of 0 μg/mL PEG_4-EKGPDP, color development could not be generated, indicating that the blocking process was successfully accomplished. When 20, 40 and 60 μg/mL PEG_4-EKGPDP were immobilized on the sensing surface, saturation signal of the color development was observed, indicating that the color development no longer increased. Considering that color development should be induced with an absorbance of at least 1.5 to successfully absorb the red light of the pattern in the signal guide, the color produced under this condition was insufficient; therefore, a higher concentration of PEG_4-EKGPDP had to be immobilized on the sensing surface. As shown in Figs. 3A and S3, since the difference in color development between 80 and 100 μg/mL PEG_4-EKGPDP was not significant, we assumed that a sufficiently strong color development could be induced using 80 μg/mL PEG_4-EKGPDP. Therefore, the concentration of PEG_4-EKGPDP immobilized on the

sensing surface was optimized at 80 μg/mL. In addition, it is important to optimize the reaction time as well as to increase the sensitivity, because an enzyme-based chromogenic reaction is used in this study. In an enzymatic reaction, saturation of the signal occurs at all concentrations if the reaction time is too long. Conversely, if the reaction time is too short, it is not easy to identify a signal that corresponds to the concentration. Therefore, the TMB reaction time should be optimized. As shown in Figs. 3A and S3, for a reaction time of 10 min, the absorbance of the induced color development exceeds 1.5, which can cause the pattern of the signal guide to disappear. Increasing the concentration of the antibodies immobilized on the sensing surface can reduce the reaction time, but considering the economics of POCT, we thought that it is better to decrease the concentration of the antibodies used in the reaction and to increase the reaction time. Based on these results, the TMB reaction time was set to 10 min, as the color development due to the chromogenic reaction was sufficient under this condition.

Next, the uCTX-II assay was performed by applying the optimized PEG_4-EKGPDP concentration to the antigen-antibody mixture (uCTX-II: HRP-Ab(100X) = 1:3) used in a previously reported study (Han et al., 2014; Park et al., 2017). However, a notable difference in color-development was not detected among the uCTX-II concentration because the blue product by the chromogenic reaction was excessively generated at 10 ng/mL uCTX-II. This result indicates that, a substantial amount of HRP-Ab could react with PEG_4-EKGPDP even after reacting with uCTX-II, because the HRP-Ab concentration is too high compared to the uCTX-II concentration. Therefore, the conditions were changed by adjusting the dilution rate of HRP-Ab and the ratio between uCTX-II and HRP-Ab so that the concentration of uCTX-II was relatively high. The optimization test for the antigen and antibody ratio was performed for four instances using 0 and 10 ng/mL uCTX-II (Fig. 3B and C). As shown in the figure, condition B(a) resulted in the most significant color difference for uCTX-II concentrations of 0 and 10 ng/mL; however, the intensity of color development at 0 ng/mL was not sufficient to eliminate the red pattern in the signal guide. For condition C(a), the color difference was not significant at uCTX-II concentrations of 0 and 10 ng/mL. However, there was a clear difference in the color development between 0 and 10 ng/mL uCTX-II under conditions B(b) and C(b). Among these conditions, since condition C(b) caused a sufficient color development while using fewer antibodies in the uCTX-II immunoassay, this condition was selected as the final condition for subsequent uCTX-II analysis.

3.4. Verification of the optical filtration principle for quantitative analysis

In the developed chromogen-based optical filtration principle, the light intensity of the signal guide on the paper, that was observed via the

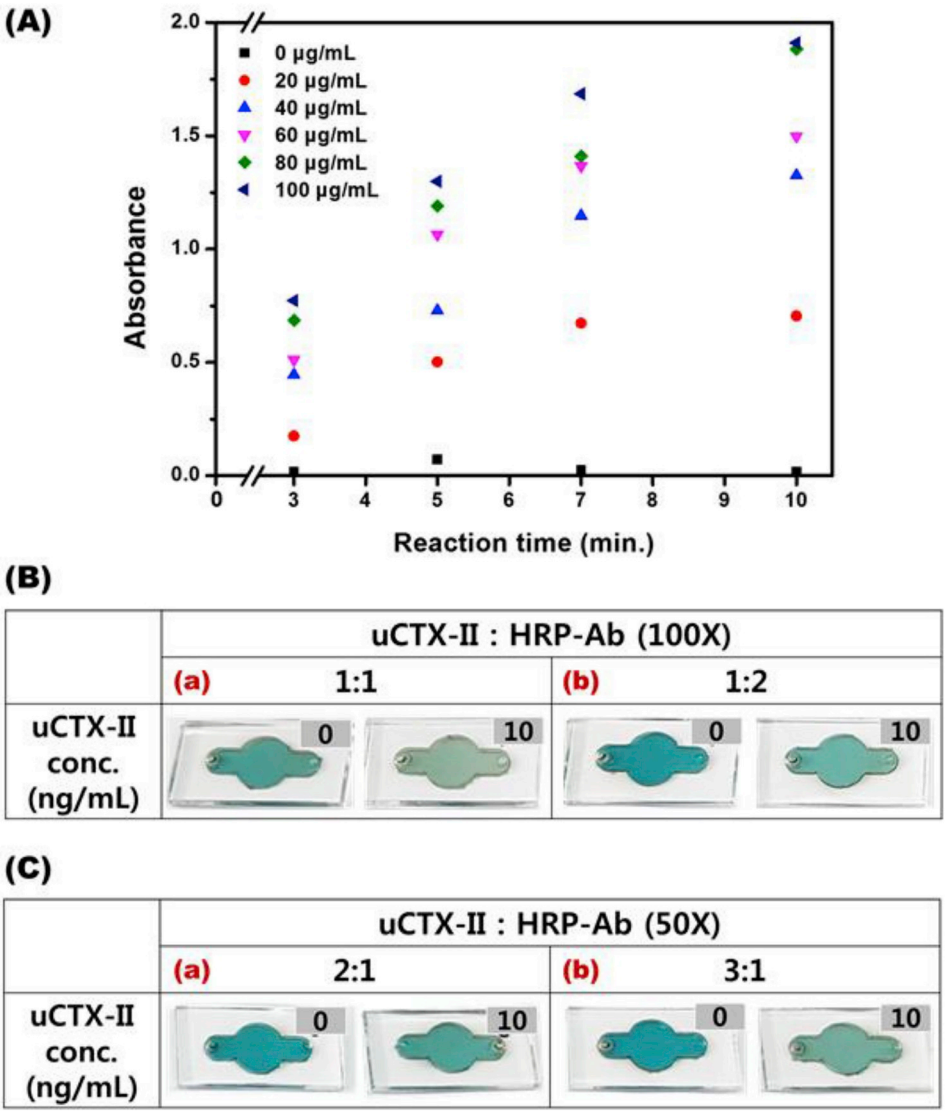

Fig. 3. Absorbance measurement for optimization of the PEG_4-EKGPDP concentration and the TMB reaction time. TMB reaction time was adjusted for 3, 5, 7 and 10 min. The absorbance measured at 652 nm was compared based on PEG_4-EKGPDP concentration and the TMB reaction time (A). The acquired images for the optimized ratio of uCTX-II to HRP-Ab. HRP-Ab was diluted (B) 100-fold or (C) 50-fold to confirm the difference in the color development depending on the presence or absence of uCTX-II. (For interpretation of the references to color in this figure legend, the reader is referred to the Web version of this article.)

biosensing channel, is closely related to the amount of blue-colored product generated by the enzymatic catalytic reaction in the biosensing channel. The amount of the blue-colored product is proportional to the injected uCTX-II concentration. Therefore, to confirm the correlation between changes in the color intensity of the signal guide in combination with the changes in uCTX-II concentration, various concentrations of uCTX-II (0, 2.5, 5, 7.5 and 10 ng/mL) were prepared and evaluated using the HRP-TMB-based immunoassay. Since the uCTX-II, which is used as a target molecule, has a monomeric epitope, the competitive immunoassay method was employed to accurately quantify the uCTX-II. To perform this experiment, the biosensing channel was modified with antigen analogs (PEG_4-EKGPDP) and the cocktail solution with HRP-Ab and uCTX-II antigen was utilized, followed by the TMB solution. According to the competitive immunoassay principle, the amount of the HRP-Ab that reacted with the PEG_4-EKGPDP is inversely proportional to the concentration of the applied-uCTX-II. Thus, the amount of the generated blue-color product is also inversely proportional to the quantity of uCTX-II.

As shown in Fig. 4A, the developed color intensity in the biosensing channel was inversely proportional to the uCTX-II concentration due to the competitive immunoassay principle. To clearly demonstrate the changes in the optical intensity based on the chromogen concentration, the spectral characteristics of the light transmitted through the biosensing channel that induced color development according to the various concentrations of uCTX-II was measured using a spectrophotometer. Fig. 4B shows that the absorbance gradually decreased according to the increase of uCTX-II, indicating that the HPR-TMB-based blue-colored product specifically absorbs 652 nm wavelength that is associated with the red-light region. Considering that the signal guide is designed to reflect red color of different intensities, it can be confirmed that the biosensing channel that induces the color-development from the enzyme-based chromogenic reaction can be used as an optical filter. This is because the biosensing channels have a different absorption rate for red light. Based on the acquired test results, we conclude that the HRP-TMP-based immunoassay could be integrated with the developed smartphone-based biosensing platform.

3.5. Quantitative analysis of uCTX-II using a smartphone and a paper-based signal guide

To verify the applicability of the developed biosensing principle, uCTX-II was measured using a smartphone and the designed paper-based signal guide. To incorporate uCTX-II analysis to the developed smartphone-based biosensing platform, a smartphone gadget was fabricated that consisted of a prism, channel holder, dispersion film and cover (Fig. 5A).

The prism was used to refract light so that the signal guide image could be focused on the lens of the smartphone camera. The channel holder was used to fix the channel on the prism and the dispersion film allowed the light generated by the smartphone flash to spread uniformly within the smartphone gadget. To minimize the influence of external light, a cover was used to obtain accurate images under light-tight conditions. Using the developed smartphone gadget, uCTX-II analysis was performed. As shown in Fig. 5C (upper), in the absence of uCTX-II, the pattern was not observed due to the maximum development of blue color that can maximally absorb red light. The number of observed red patterns gradually increased according to the applied concentration of uCTX-II and the configuration of red patterns in the signal guide was clearly observed, indicating that the introduced biosensing principle integrated with a smartphone was effective. Although the number of observed red patterns in the signal guide could be counted using the developed smartphone-based biosensing platform, the results are likely to be influenced by the subjective intervention of individual observers. Therefore, to provide the accuracy of the developed biosensor by objectifying the number of observed red patterns, the acquired images were analyzed and calculated using a sketch filter effect that has a pattern-recognition option (Fig. 5B). Using this sketch filter effect, the numbers of residual red patterns observed at 0, 2.5, 5, 7.5 and 10 ng/mL

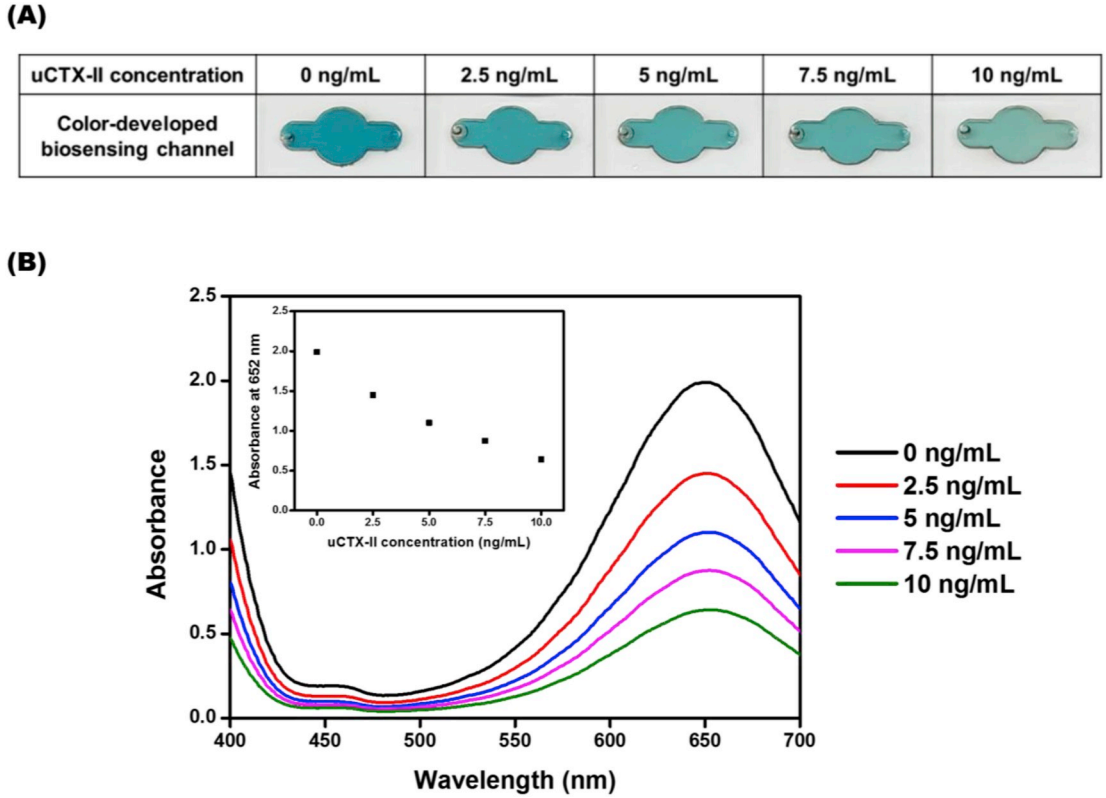

Fig. 4. The result images of the biosensing channel (A) and absorbance measurement (B) according to the uCTX-II concentration.

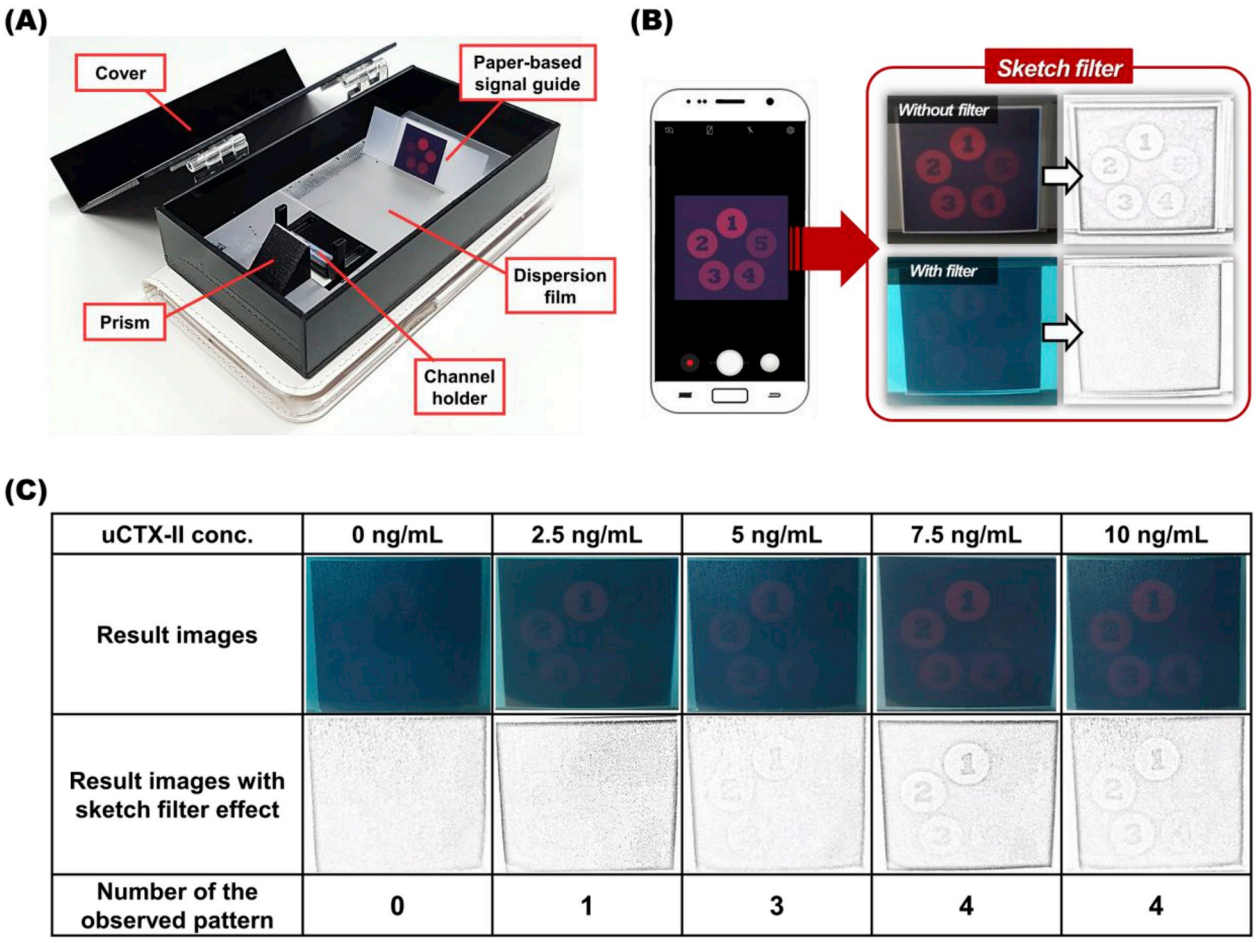

uCTX-II conc.	0 ng/mL	2.5 ng/mL	5 ng/mL	7.5 ng/mL	10 ng/mL
Result images					
Result images with sketch filter effect					
Number of the observed pattern	0	1	3	4	4

Fig. 5. (A) Configuration of the smartphone gadget for the count-based analysis. This instrument is composed of a prism, channel holder, dispersion film, paper-based signal guide and cover. (B) Image processing using a sketch filter of the smartphone to obtain clearer images. (C) Result images of the uCTX-II measurement using a smartphone. After applying the sketch filter to each image, the number of the observed patterns was counted.

uCTX-II in the sample were 0, 1, 3, 4 and 4, respectively (Fig. 5C (middle and bottom), demonstrating a high correlation with the naked-eye detection without the sketch filter effect. To verify the reproducibility of the assay, tests were performed at least five times by applying buffer-spiked uCTX-II samples under the optimized condition (reaction time, temperature, and pH). As shown in Fig. S4, the results from tests were identical to Fig. 5C, indicating that the developed biosensing method possesses high reproducibility.

3.6. Quantitative analysis of the uCTX-II using artificial urine

Based on the aforementioned results, it was demonstrated that the developed biosensing system could be used for quantitative analysis of uCTX-II under buffer conditions. However, to use the developed sensing system as a POCT biosensor, it is not only possible to measure the uCTX-II present in a buffer, but to also accurately measure the concentration of uCTX-II present in real urine samples. Therefore, to confirm the applicability of the developed biosensing system to real samples, artificial urine solution (AUS) with the same composition as real urine was prepared. The AUS is comprised of various substances (calcium chloride, magnesium chloride, sodium chloride, sodium sulfate, sodium citrate, sodium oxalate, potassium phosphate, potassium chloride, ammonium chloride, urea, creatine and tryptic soy broth) (Prywer et al., 2018). This solution was spiked with five different concentration of uCTX-II (0, 2.5, 5, 7.5 and 10 ng/mL) and these samples were injected and analyzed.

As shown in Fig. 6A, when the developed biosensor was used as an analyzer, the number of observed red patterns increased in accordance with the increase in the concentration of uCTX-II. The acquired images were also analyzed and calculated based on a sketch filter effect to provide the accuracy of the developed biosensing system. As a result, the number of calculated red patterns was recorded as 0, 1, 3, 3 and 4 for the uCTX-II detection range of 0–10 ng/mL. This exhibited high similarity to the results obtained using the buffer solution. These results indicate that the various substances present in the solution do not affect the reaction between the uCTX-II antigen and antibody, demonstrating that the developed system can be applied to real urine samples. In particular, when the uCTX-II concentration is 0 ng/mL, all red patterns are absent, indicating that the developed system can clearly distinguish between osteoarthritis patients and healthy persons.

To determine whether the concentration of uCTX-II can be quantitatively analyzed using the urine sample of patients suffering from diabetic and renal failure complications, glucose-spiked AUS and albumin-spiked AUS were prepared and analyzed as previously described. In general, given that the kidney can return filtered glucose back to the bloodstream, urine does not contain glucose. In diabetic patients, however, glucose with a concentration in excess of 0.8 mM is released from urine. As such, 1 mM glucose-spiked AUS was selected and used in this study. Fig. 6B represents the result of the analysis of glucose-spiked AUS. The number of observed red patterns was calculated as 0, 1, 2, 3 and 4, for uCTX-II concentration from 0 to 10 ng/mL, confirming that there is a high correlation with AUS results. These results show that the developed biosensing system can also be applied to diabetic patients care. Fig. 6C represents the result of the analysis of albumin-spiked AUS. When the kidney function is abnormal, since the albumin at 30 mg/g

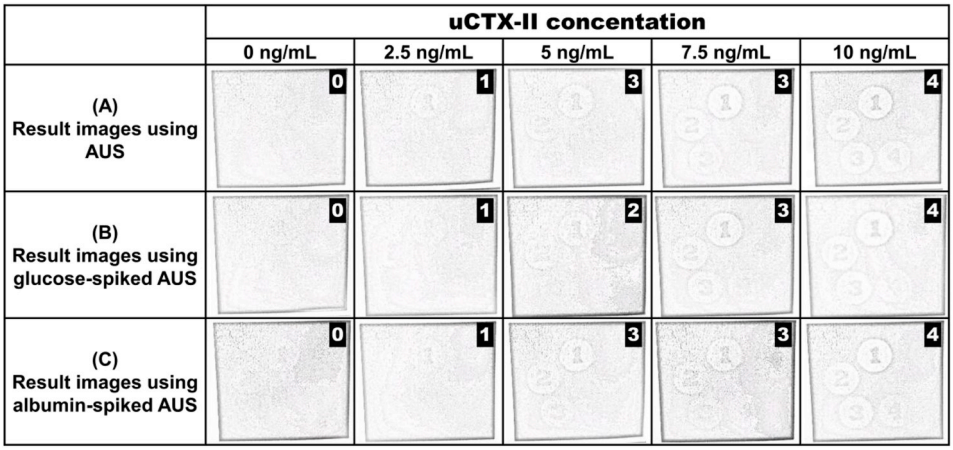

Fig. 6. The results of the quantitative analysis of uCTX-II using (A) artificial urine solution (B) glucose-spiked artificial urine solution (C) albumin-spiked artificial urine solution.

creatinine is excreted via the urine, 50 mg/g creatinine-spiked AUS was selected and utilized in this study. As shown in Fig. 6C, the number of calculated red patterns observed in the range of 0–10 ng/mL uCTX-II were 0, 1, 3, 3 and 4 for the samples. These results are highly correlated with the results obtained using the AUS and glucose-spiked AUS, indicating that it is applicable to patients with renal failure complications. In addition, the registered detection range of uCTX-II was found to fully cover the clinical range of uCTX-II (0–10 ng/mL) for OA diagnosis and/or prognosis (Garnero et al., 2003).

Based on these results, it was confirmed that quantitative analysis of uCTX-II present in the urine of diabetic and renal failure patients, as well as real human urine samples, could be achieved using the developed biosensor system.

4. Conclusions

In this study, we developed an optical biosensing system using a smartphone and very simple components. Since all sensing processes, such as signal acquisition and interpretation, were performed using a single tool (i.e. a smartphone), the developed system is user-friendly and easy to operate. The use of a paper-based signal guide yielded additional advantages including high cost-effectiveness and productivity. In addition, the count-based analysis method based on selective light absorption and the specific wavelength filtering phenomenon was used in the developed biosensing system. Therefore, an intuitive measurement of uCTX-II (0–10 ng/mL) could be accomplished by simply counting the number of observed patterns of the signal guide and the developed biosensing system could be applied to the analysis of real urine samples. Additionally, this system uses the HRP-mediated chromogenic reaction, which is often employed for biochemical analysis. As such, it can be applied to the detection of other target analytes. Based on our results, we expect that the developed biosensing system is potentially applicable in POCT equipment in various fields.

Declaration of competing interest

The authors declare that they have no known competing financial interests or personal relationships that could have appeared to influence the work reported in this paper.

CRediT authorship contribution statement

Saemi Kim: Writing - original draft, Conceptualization, Methodology, Investigation, Formal analysis, Data curation. **Hyeong Jin Chun:** Writing - original draft, Conceptualization, Methodology, Investigation, Formal analysis, Data curation. **Kyung Won Lee:** Methodology, Investigation, Formal analysis, Data curation. **Hyun C. Yoon:** Writing - original draft, Conceptualization, Validation, Supervision, Project administration.

Acknowledgements

This work was supported by the Creative Materials Discovery Program (NRF-2019M3D1A1078943) and the Priority Research Centers Program (NRF-2019R1A6A1A11051471) funded by the National Research Foundation of Korea (NRF). We also acknowledge the support from the Technology Innovation Program (10051409) funded by the Ministry of Trade, Industry and Energy (MOTIE, Korea).

Appendix A. Supplementary data

Supplementary data to this article can be found online at https://doi.org/10.1016/j.bios.2019.111932.

References

Birmingham, J.D., Vilim, V., Kraus, V.B., 2006. Biomark. Insights 1, 61–76.
Chun, H.J., Han, Y.D., Park, Y.M., Kim, K.R., Lee, S.J., Yoon, H.C., 2018. Materials 11, 388.
Chun, H.J., Park, Y.M., Han, Y.D., Jang, Y.H., Yoon, H.C., 2014. Biochip J. 8, 218–226.
Coleman, B., Coarsey, C., Kabir, M.A., Asghar, W., 2019. Sens. Actuators B. 282, 225–231.
Coskun, A.F., Wong, J., Khodadadi, D., Nagi, R., Tey, A., Ozcan, A., 2013. Lab Chip 13, 636–640.
Eyre, D.R., Weis, M.A., Wu, J.-J., 2008. Methods 45, 65–74.
Garnero, P., Conrozier, T., Christgau, S., Mathieu, P., Delmas, P.D., Vignon, E., 2003. Ann. Rheum. Dis. 62, 939–943.
Garnero, P., Peterfy, C., Zaim, S., Schoenharting, M., 2005. Arthritis Rheum. 52, 2822–2829.
Guo, J., 2016. Anal. Chem. 88, 11986–11989.
Guo, J., 2017. Anal. Chem. 89, 8609–8613.
Guo, J., Ma, X., 2017. Biosens. Bioelectron. 94, 415–419.
Han, Y.D., Chun, H.J., Yoon, H.C., 2014. Biosens. Bioelectron. 29, 259–268.
Huang, X., Xu, D., Chen, J., Liu, J., Li, Y., Song, J., Ma, X., Guo, J., 2018. Analyst 143, 5339–5351.
Kang, B.-H., Park, M., Jeong, K.-H., 2017. Biochip J. 11, 294–299.
Kim, J.-H., Joo, H.-G., Kim, T.-H., Ju, Y.-G., 2015. Biochip J. 9, 285–292.
Kim, S.J., Park, Y.M., Min, B.H., Lee, D.S., Yoon, H.C., 2013. Biochip J. 7, 399–407.
Klostranec, J.M., Chan, W.C.W., 2006. Adv. Mater. 18, 1953–1964.
Kong, S.Y., Stabler, T.V., Criscione, L.G., Elliott, A.L., Jordan, J.M., Kraus, V.B., 2006. Arthritis Rheum. 54, 2496–2504.
Lee, H., Dellatore, S.M., Miller, W.M., Messersmith, P.B., 2007. Science 318, 426–430.
Mabey, D., Peeling, R.W., Ustianowski, A., Perkins, M.D., 2004. Nat. Rev. Microbiol. 2, 231–240.
Ozcan, A., 2014. Lab Chip 14, 3187–3194.
Park, Y.M., Han, Y.D., Chun, H.J., Yoon, H.C., 2017. Biosens. Bioelectron. 93, 205–211.
Park, Y.M., Han, Y.D., Kim, K.R., Zhang, C., Yoon, H.C., 2015. Anal. Methods 7, 6437–6442.
Peeling, R.W., Mabey, D., 2010. Clin. Microbiol. Infect. 16, 1062–1069.
Prywer, J., Kozanecki, M., Mielniczek-Brzóska, E., Torzewska, A., 2018. Crystals 8, 164.

Reijman, M., Hazes, J.M.W., Bierma-Zeinstra, S.M.A., Koes, B.W., Christgau, S., Christiansen, C., Uitterlinden, A.G., Pols, H.A.P., 2004. Arthritis Rheum. 50, 2471–2478.
Shen, L., Hagen, J.A., Papautsky, I., 2012. Lab Chip 12, 4240–4243.
Soni, A., Surana, R.K., Jha, S.K., 2018. Sens. Actuators B. 269, 346–353.
Szili, E.J., Jane, A., Low, S.P., Sweetman, M., MacArdle, P., Kumar, S., Smart, R.S.C., Voelcker, N.H., 2011. Sens. Actuators B. 160, 341–348.
Tatzber, F., Griebenow, S., Wonisch, W., Winkler, R., 2003. Anal. Biochem. 316, 147–153.
Uys, P.W., Warren, R., van Helden, P.D., 2009. J. Clin. Microbiol. 47, 1484–1490.
Vashist, S.K., van Oordt, T., Schneider, E.M., Zengerle, R., von Stetten, F., Luong, J.H.T., 2015. Biosens. Bioelectron. 67, 248–255.
Wang, L.J., Chang, Y.C., Sun, R., Li, L., 2017. Biosens. Bioelectron. 87, 686–692.
Wei, Q., Acuna, G., Kim, S., Vietz, C., Tseng, D., Chae, J., Shir, D., Luo, W., Tinnefeld, P., Ozcan, A., 2017. Sci. Rep. 7, 2124.
Xie, W., Lei, L., Tian, M., Zhang, Z., Liu, Y., 2018. Analyst 143, 2901–2907.
Xu, D., Huang, X., Guo, J., Ma, X., 2018. Biosens. Bioelectron. 110, 78–88.
Yang, X., Sun, M., Wang, T., Wong, M.W., Huang, D., 2019. Sens. Actuators B. 283, 524–531.
Yu, H., Tan, Y., Cunningham, B.T., 2014. Anal. Chem. 86, 8805–8813.
Zeng, F., Duan, W., Zhu, B., Mu, T., Zhu, L., Guo, J., Ma, X., 2019. Anal. Chem. 91, 1064–1070.
Zeng, F., Mou, T., Zhang, C., Huang, X., Wang, B., Ma, X., Guo, J., 2019. Analyst 144, 137–142.